SCIENTIFIC REPORTS

Correction: Author Correction

OPEN

Radioligand binding analysis of α_2 adrenoceptors with [11C]yohimbine in brain in vivo: Extended Inhibition Plot correction for plasma protein binding

Jenny-Ann Phan[1,2,3], Anne M. Landau[2,4], Steen Jakobsen[2], Dean F. Wong[5] & Albert Gjedde [6,7,8,9,10]

We describe a novel method of kinetic analysis of radioligand binding to neuroreceptors in brain *in vivo*, here applied to noradrenaline receptors in rat brain. The method uses positron emission tomography (PET) of [11C]yohimbine binding in brain to quantify the density and affinity of α_2 adrenoceptors under condition of changing radioligand binding to plasma proteins. We obtained dynamic PET recordings from brain of Spraque Dawley rats at baseline, followed by pharmacological challenge with unlabeled yohimbine (0.3 mg/kg). The challenge with unlabeled ligand failed to diminish radioligand accumulation in brain tissue, due to the blocking of radioligand binding to plasma proteins that elevated the free fractions of the radioligand in plasma. We devised a method that graphically resolved the masking of unlabeled ligand binding by the increase of radioligand free fractions in plasma. The Extended Inhibition Plot introduced here yielded an estimate of the volume of distribution of non-displaceable ligand in brain tissue that increased with the increase of the free fraction of the radioligand in plasma. The resulting binding potentials of the radioligand declined by 50–60% in the presence of unlabeled ligand. The kinetic unmasking of inhibited binding reflected in the increase of the reference volume of distribution yielded estimates of receptor saturation consistent with the binding of unlabeled ligand.

Deficient noradrenergic neurotransmission is implicated in a spectrum of brain disorders, including neuro-degenerative and psychiatric disorders. Locus coeruleus is the major source of neuronal terminals engaged in noradrenaline synthesis, and pathological protein deposition together with loss of neurons at this site has been described in Alzheimer's disease[1]. Similarly, attenuated levels of noradrenaline have been reported in Parkinson's disease[2]. Attenuated noradrenergic activity is implicated in major depression, as indicated by findings of depleted noradrenaline in depressed patients with rapidly worsening symptoms[3]. Thus, multiple post-mortem studies have revealed elevated α_2 adrenoceptor expression in suicide victims with a retrospective diagnosis of major depression, with upregulation of the α_{2A} adrenoceptor subtype noted particularly in the frontal and prefrontal cortices[4–6].

Increased α_2 adrenoceptor density is believed to compensate for attenuated noradrenaline release when experimental depletion of brain noradrenaline in rats led to upregulated cortical l α_2 adrenoceptors[7]. In brains of

[1]Department of Biomedicine, Aarhus University, Aarhus, 8000, Denmark. [2]Department of Nuclear Medicine and PET centre, Aarhus University Hospital, Aarhus, 8000, Denmark. [3]Department of Radiology & Radiological Science, Johns Hopkins University Hospital, Baltimore, 21231, USA. [4]Translational Neuropsychiatry Unit, Aarhus University Hospital, Aarhus, 8240, Denmark. [5]Radiology, Psychiatry, Neuroscience, Neurology, Environmental Health Sciences, Johns Hopkins University, Johns Hopkins Medical Institutions, JHOC Bldg room 3245, 601 N. Caroline St., Baltimore MD, 21287, USA. [6]Department of Neuroscience, University of Copenhagen, Copenhagen, 2200, Denmark. [7]Department of Neurology and Neurosurgery, McGill University, Montréal, Québec, Canada. [8]Neurosciences Research Center, Tabriz University of Medical Science, Tabriz, Iran. [9]Department of Nuclear Medicine, Odense University Hospital, Odense, 5230, Denmark. [10]Department of Clinical Medicine, University of Southern Denmark, Odense, 5230, Denmark. Correspondence and requests for materials should be addressed to A.G. (email: gjedde@sund.ku.dk)

patients who suffered from bipolar disorder, lower tyrosine hydroxylase immunoreactivity was found in locus coeruleus, consistent with deficient noradrenaline synthesis[8]. In support of low noradrenaline, a more recent PET study showed lower occupancy of noradrenaline transporters in locus coeruleus in patients with bipolar disorder or major depression, compared to healthy controls[9]. In attention-deficit/hyperactivity disorder (ADHD), impulsive behavior was associated directly with low noradrenergic tone[10].

Central noradrenaline is known to modulate cognitive functions, such as arousal, mood, learning and memory (reviewed by Sara *et al.*[11]). To understand the neurobiology underlying brain disorders in the living brain, non-invasive PET using selective ligands can be used to monitor the activity of neurotransmission as a sign of disease severity and response to pharmacological therapy. The labeling of yohimbine with carbon-11 provided new opportunities to measure noradrenergic transmission in pathological conditions. [11C]yohimbine so far has been applied to image α_2 adrenoceptor *in vivo* in different species, including humans[12], pigs[13,14], and rats[15–17]. However, the wide anatomical distribution of noradrenergic receptors complicates the quantification of receptor occupancy and receptor density.

The aims of the present study are twofold: First, we use yohimbine to obtain an estimate of the reference distribution volume of the radioligand in the absence of a true anatomical reference region. Second, we use kinetics to resolve the masking of ligand binding competition by pharmacological challenge that raises the plasma-free fraction of the radioligand.

Protein binding of drugs in plasma are of special interest in pharmacological studies because only the drug that is unbound to plasma proteins (i.e., is "free") has access to target tissue and hence is biological active[18]. PET imaging of the brain with radiolabeleld ligands faces the same issue because the blood-brain barrier (BBB) permeability of the drug depends on the free-fraction of the ligand among many other factors. The CSF/plasma albumin ratio is 0.006, indicating that only a negligible fraction of albumin passes the BBB[19]. *In vitro*, the free drug concentration depends on factors such as protein quantity, drug affinity, and total drug concentration, while *in vivo*, factors such as metabolism, excretion and membrane transport, all influence the free drug concentration.

Quantification of neuroreceptor density with PET requires the determination of receptor availability at two or more different levels. The number of receptors available for radioligand binding can be modulated by agents that induce release or depletion of endogenous neurotransmitters, or by introduction of exogenous molecules that either bind to the receptors or affect the mechanism of binding of the endogenous ligands. Thus, pharmacological modulation changes the availability of sites for radioligand binding. Commonly, modulation of occupancy is achieved with unlabeled exogenous ligands that compete at the binding site. Receptor occupancy and density are then calculated from the fractional change of the receptor availability (also known as binding potential) after the pharmacolcgcial challenge.

To determine the binding potential, it is necessary to know the total volume of distribution of all labeled molecules in the tissue, V_T, and the volume of distribution of molecules that cannot be displaced from binding (i.e., the volume of distribution indicative of "non-displaceable" binding), represented as V_{ND}[20,21]. For radioligands that bind to some regions only (as in the case of dopaminergic radioligands), estimates of V_{ND} are the volumes of distribution in brain regions with no specific binding (reference regions). In contrast, for radioligands distributed in the entire brain, a reference volume must be estimated from regional values of V_T at two different different degrees of receptor occupancy, as described in Methods below.

Changes of free fractions of tracer in plasma, f_P, do not perturb the calculation of binding potentials in the presence of a non-binding reference region, because the value of V_{ND} is obtained from the degree of non-displaceble binding in the reference region, which scales with the freely distributed ligand in plasma. In the absence of a non-binding reference region, changes of f_P influence the magnitudes of V_T and V_{ND} estimates and hence may mask the competition from a blocking agent.

Here, we demonstrate a novel solution to issue of elevation of the magnitude of f_P in response to pharmacological challenge that may occur *in vivo*. The mathematical approach is designed to resolve the masking of competition attributable to the decreased protein binding of the tracer in plasma. As an example, we quantified the binding of [11C]yohimbine to widely distributed α_2 adrenoceptors in the rat brain by an analysis that is not limited to α_2 adrenoceptors but can be applied to radioligands of other receptors that lack a non-binding reference region.

Results

Tracer Accumulation as a Function of Time. To evaluate the pattern of [11C]yohimbine binding to α_2 adrenoceptors, we examined the binding at two levels of receptor occupancy, at baseline and at challenge with unlabeled yohimbine (0.3 mg/kg) administered as an i.v. bolus. The average time-activity curves (TACs) in plasma and brain regions show the kinetic behavior of [11C]yohimbine as it accumulates in the tissue (Fig. 1B). The clearance of the radioligand from the circulation occurred rapidly within the first 10 min after intravenous bolus injection. The uptake in cerebellum peaked at 10 min post-injection, while the accumulation peaked later in other brain regions at 20 min. TAC of the unlabeled yohimbine challenge revealed prominently elevated early uptake compared to baseline, showing that the effect of the challenge is not apparent exclusively from the TACs.

Increased K_1 May Indicate Displacement of Plasma Protein Binding. As for the trends of TACs, the magnitude of unidirectional clearance from plasma to brain tissue, represented by K_1, was markedly elevated in the challenge condition. The value of K_1 at the challenge rose initially and maintained higher values during the time of acquisition than in the baseline (Fig. 2A). The magnitude of the fractional clearance from brain to plasma, symbolized by k_2', likewise was higher in the challenge than in the baseline condition, to the same relative extent as the value of K_1 (Fig. 2B). The ratio of the the estimates of K_1 and k_2' remained similar throughout the acquisition in both conditions (Fig. 2C). The increased values of K_1 and k_2' in response to yohimbine challenge are the results of two opposite effects, one the blocking at α adrenoceptor sites by unlabeled yohimbine that underlies the
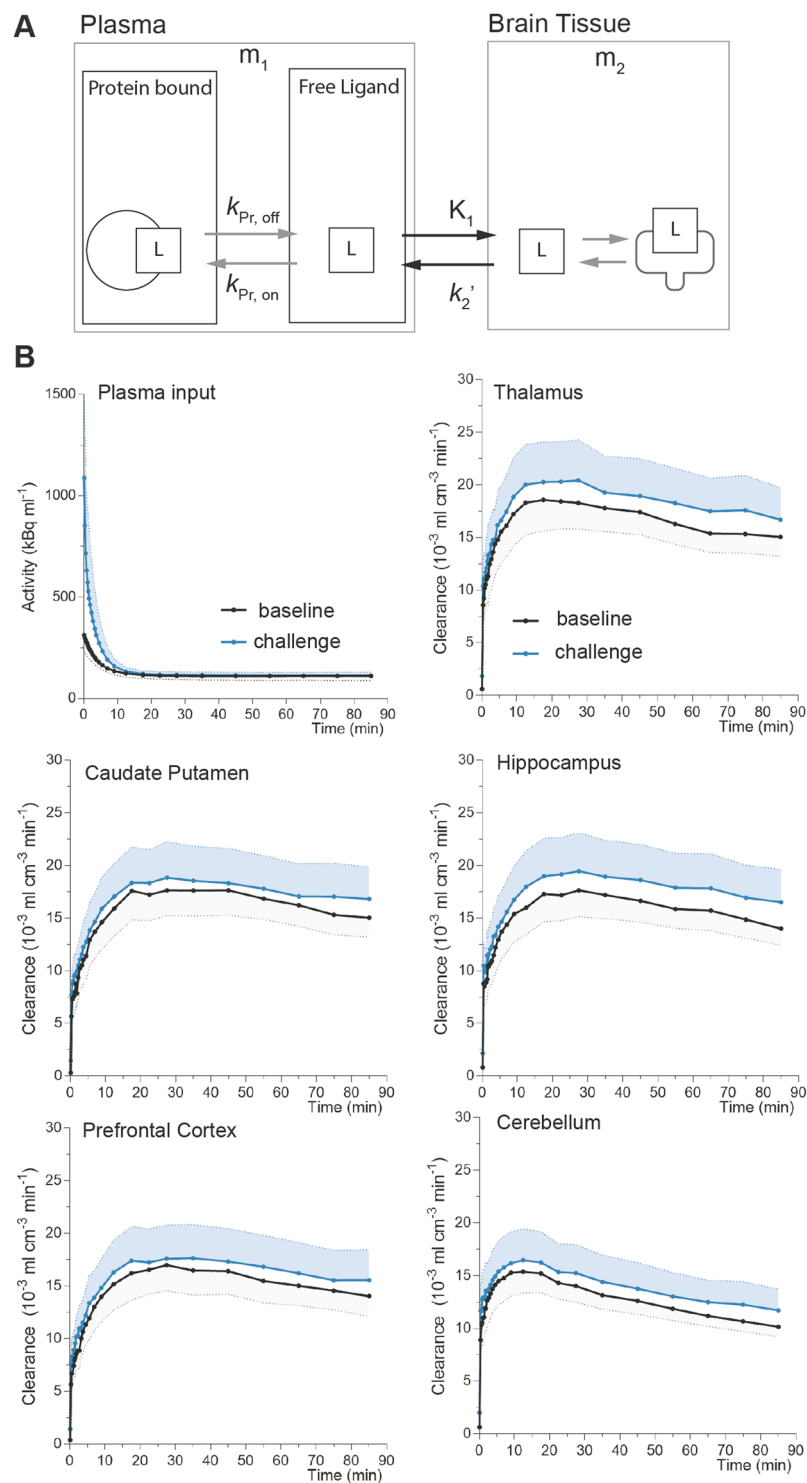
Figure 1. Tracer Accumulation as a Function of Time. Panel (A) illustrates the one-tissue compartment model used for data analysis. In this model, K_1 represents the clearance from plasma to brain tissue while k_2' represents the fractional clearance of ligand from brain to plasma. Here, the free amount of ligand in plasma reflects the exchangeable compartment when only the unbound ligand crosses the BBB and enters brain tissue. The magnitude of K_1 depends on the free concentration in plasma, cerebral blood flow, and the permeability surface area as well as the association and dissociation constants for plasma protein binding (depicted here as $k_{pr,on}$ and $k_{pr,off}$). The magnitude of k_2' depends on the concentration of ligand in brain tissue and the association and disassociation constants for receptor binding (shown as grey arrows on the right hand side). Initial evaluation of tracer accumulation in panel (B) demonstrates that average plasma input curves are of similar magnitude, indicating that the challenge condition did not significantly alter the baseline input function. The solid curves represent the average time-activities of individual curves divided by the integral of the respective plasma input to normalize for variations attributed to differences of injected radioactive dose, body weight and other

bioavailability factors. Baseline is shown in black, yohimbine challenge in blue, and the shaded areas indicate the standard error of the mean. The time-activity curves (TACs) at challenge condition were markedly higher compared to baseline across all regions, suggesting that the inhibition effect is not immediate visible.

....

elevated value of k_2', and the other the decreased protein binding reflected in the increased estimate of f_P that accounts for the elevated value of K_1.

The early peak of V_T curves (Fig. 1C) together with the elevated K_1 (Fig. 2A) suggest that the increased values of f_P reflect the effects of protein binding blocked by an unlabeled competitor. More than 80% of yohimbine in the circulation is bound to plasma proteins[22] that renders [11C]yohimbine prone to self-displacement at plasma protein sites with increased value of f_P. The higher f_P of [11C]yohimbine in turn masks the competition from unlabeled yohimbine in the brain tissue.

To determine the degree of masking, we measured the free fractions of [11C]yohimbine at baseline and challenge conditions by means of plasma ultrafiltration in a separate group of animals. We determined the values of f_P by administration of 0.3 mg/kg yohimbine. The challenge with unlabeled ligand *ex vivo* significantly raised the value of f_P by 30% on average compared to baseline (P < 0.05) (Fig. 2D middle panel). To exclude the possibility that the elevation of f_P is due to competition from hepatic metabolism or renal elimination, we repeated the experiment *in vitro* (Fig. 2D right panel). *In vitro*, the experiments confirmed no change of the value of f_P with amphetamine challenge. As expected, the magnitude of f_P increased significantly (P < 0.001) in response to challenge with unlabeled yohimbine, in proportion to the yohimbine dose.

Extended Inhibition Plots and Binding Potentials. On the basis of the substantial change of the value of f_P shown *ex vivo* and *in vitro*, we applied the Extended Inhibition Plot to resolve the volume of distribution of non-displaceable radioligand at inhibition, $V_{ND(i)}$. In the analysis, the volume of distribution of non-displaceable radioligand at baseline, $V_{ND(b)}$, is required to determine the magnitude of $V_{ND(i)}$ at the challenge.

Previously, in the same strain of animals with same PET protocol, we confirmed that the values of $V_{ND(b)}$ and f_P did not change when [11C]yohimbine binding was challenged with amphetamine (2 mg/kg)[16], using the plasma input function. The plasma input was not metabolite corrected because data from two rats revealed no radioactive metabolites, as for radioactive metabolites in pigs[14]. Because the value of f_P remained the same with amphetamine challenge, we used the Inhibition Plot to obtain a value of $V_{ND(b)}$ of 0.286 ml cm^{-3}. The similar experiments and analyses of the previous study allowed us to apply the value of $V_{ND(b)}$ of the previous study to the present study.

The graphical analysis yielded an estimate of $V_{ND(i)}$ at 0.599 ml cm^{-3} (Fig. 3A), and the degree of saturation, s, revealed that 56% of available receptors were blocked by unlabeled yohimbine, as shown in Fig. 3B.

The quantification of V_T at the challenge condition revealed the masked effect reflected in the elevated value of f_P, as illustrated both by the parametric images (Fig. 3D) and by regional V_T estimates (Fig. 3F). To determine the real pharmacological displacement of [11C]yohimbine binding, we estimated the value of the binding potential, BP_{ND}, from the estimates of V_T and the volumes of distribution of non-displaceable ligand, $V_{ND(i)}$ and $V_{ND(b)}$, respectively. As presented in Fig. 3E,G, calculations of BP_{ND} (by eq. 37 in Methods) revealed a significant decrease of BP_{ND} by the unlabeled ligand challenge. From the regionally differential estimates of BP_{ND}, we found the highest BP_{ND} in thalamus, caudate putamen, hippocampus and cortical regions, with cerebellum and olfactory bulb at the lowest binding. The estimates of BP_{ND} decreased significantly by 50–60% on average in response to the unlabeled ligand challenge, with a consistent reduction in all animals. The estimates of V_T and BP_{ND} are listed in detail in Table 1.

Receptor Density. The values of BP_{ND} enabled us to determine the α_2 adrenoceptor density *in vivo*. As presented in Fig. 4A, we estimated values of receptor density, B_{max}, and receptor affinity ($1/K_D$) by means of Eadie-Hofstee plots. We calculated the bound quantity according to eq. 2, based on the information of the BP_{ND} and specific activity. We found the greatest receptor densities in thalamus, caudate putamen, and cortical areas, with the lowest densities in cerebellum and olfactory bulb as presented in Fig. 4B. The regional receptor densities are listed in detail in Table 2 and specific activity in Table 3.

Discussion

We characterized the binding profiles of [11C]yohimbine to α_2 adrenoceptors in rat brain, using non-invasive PET. We quantified the binding potentials and regional receptor densities by means of competition analysis. The results of the study demonstrate a significant increase in f_P in response to challenge with unlabeled yohimbine at the dose of 0.3 mg/kg. We argue that the elevation of f_P was caused by displacement of radioligand from plasma proteins, which ultimately masked the effect of the pharmacological inhibition in the brain. The masked effect is evident from estimates of V_T that reflect the total concentration in brain relative to the concentration in plasma. Furthermore, the challenge condition displayed consistently higher values of K_1 in comparison to baseline, supporting the attribution of greater clearance of [11C]yohimbine and increased magnitude of f_P due to decreased protein binding. When the magnitude of K_1 is influenced by specific biological variables, including BBB permeability, cerebral blood flow (CBF) and f_P, it is important to consider the changes of CBF a potential confound. In the challenge condition, the magnitude of K_1 may be influenced by pharmacological action of yohimbine in the cardiovascular system. In humans and pigs, yohimbine is known to reduce CBF and increase blood pressure and heart rate[14,23]. Jakobsen et al.[14] showed that CBF was unaffected by a low dose of yohimbine (0.07 mg/kg), while the higher dose (1.6 mg/kg) globally lowered CBF by 30%. In contrast, challenge with RX821002 had the opposite effect on CBF. In rats, yohimbine is known to raise blood pressure and heart rate[24], while the effect on CBF is unknown.
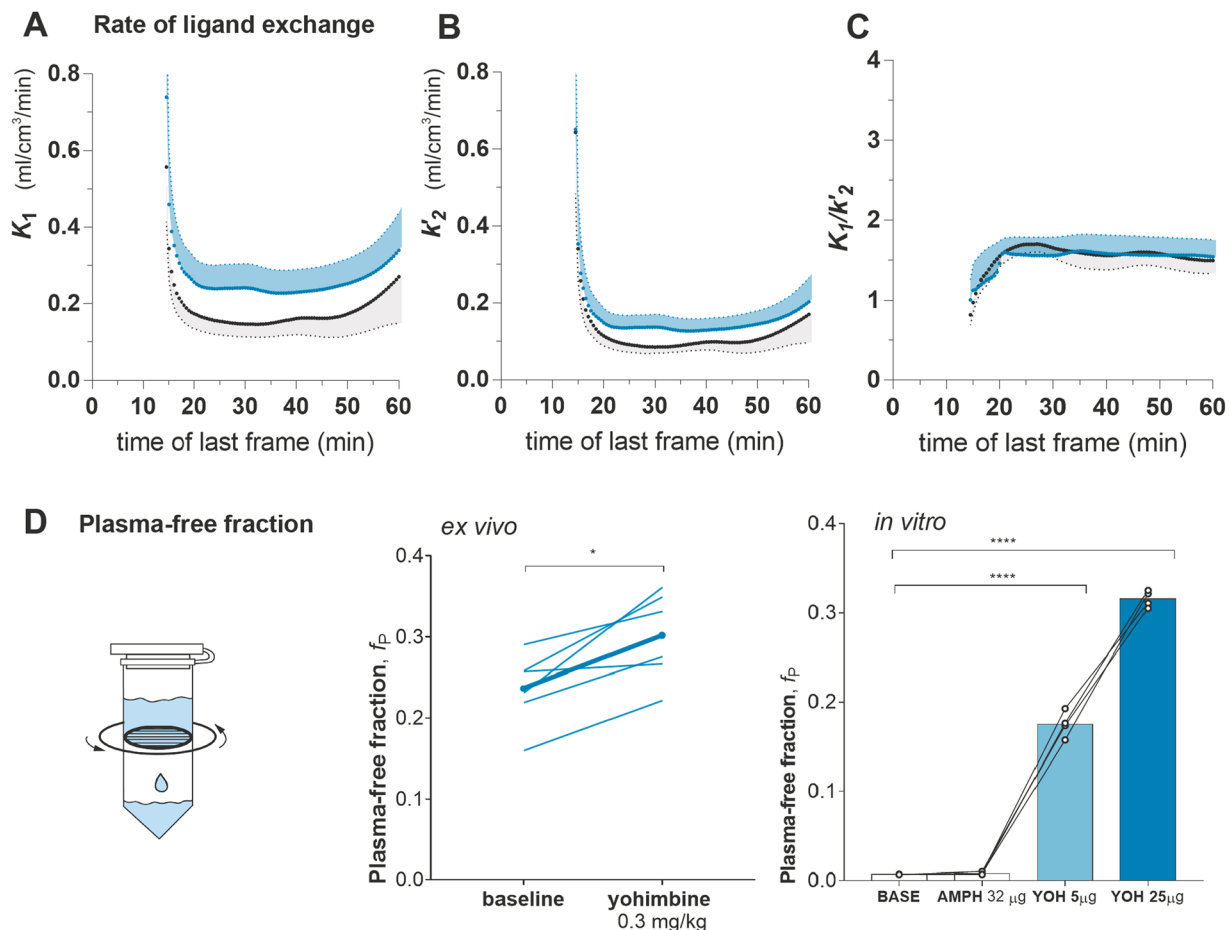
Figure 2. K_1 and k_2' as Functions of Time and Plasma Free Fractions Determined in Separate Groups. The clearance from plasma to brain, K_1 (panel (A)), and the fractional clearance from brain to plasma, k_2' (panel (B)), were calculated as functions of time using iterative analysis where each point represents a time duration of 14.5 minutes. Estimates of K_1 and k_2' from were plotted against the time of the last frame of linearization, baseline in black, and yohimbine challenge in blue, with the shaded areas indicating the standard error of the mean. Both K_1 and k_2' estimates were markedly higher in the challenge than in the baseline condition. Elevated k_2' in the challenge condition indicates displacement on α_2 adrenoceptor sites due to competition with unlabeled yohimbine, whereas increased K_1 suggest that more free ligand crosses BBB in the challenge condition due to displacement of plasma protein binding. Because of two simultaneous opposite effects, the ratio of K_1/k_2' at challenge condition (**C**) was at the same magnitude as baseline. This supports that yohimbine challenge was masked by elevated f_P. To confirm this notion, we measured f_P by means of plasma ultrafiltration (**D**) in a separate group of animals. In the *ex vivo* setup (D middle), 0.3 mg/kg yohimbine administered i.v. resulted in a significant increase of f_P by 30% as compared to baseline (P < 0.05). In the *in vitro* study, plasma was drawn before amphetamine or yohimbine were added to the samples. This showed that amphetamine did not change f_P, whereas yohimbine challenge produced a dose-dependent increase. Both low dose and high dose challenge increased f_P significantly as compared to baseline (****P < 0.0001). The thick line in D (middle) represents the group average, and the thin lines show estimates in individual animals, which connect estimates at baseline and challenge in the same animals.

The estimate of K_1 was 0.2 ml/cm³/min, corresponding to a rate of escape of 0.167 s⁻¹ for a vascular volume of 0.02 of 0.02 ml/cm³ [25]. Because there are two connected processes (escape from plasma protein binding and exchange across BBB), it is important to note that blood-brain transfer can be affected by the dynamics of protein binding (here symbolized by $k_{Pr,on}$ and $k_{Pr,off}$). When the rate of relaxation from the plasma protein binding is greater than the exchange of tracer across the BBB, the loss of ligand bound to plasma proteins is likely to keep pace with the transfer of the tracer to brain tissue. If so, the transfer across BBB must depend on the original fraction of unbound ligand in plasma, including the unlabeled challenger. The kinetics of yohimbine relaxation from albumin is not known, but the relaxation of bilirubin from plasma proteins was estimated to occur at the rate of 0.6 s⁻¹ [26]. If we assume that yohimbine leaves plasma protein binding at a rate similar to that of bilirubin, the free and bound yohimbine pools in brain vasculature are likely to maintain a constant ratio.

Another consideration is the perturbation of hepatic enzymatic clearance of [¹¹C]yohimbine in the presence of unlabeled yohimbine at the challenge dose. However, inhibited elimination by peripheral organs is an unlikely explanation for the rise of the value of f_P, when the *in vitro* assay eliminates effects of peripheral organs. The
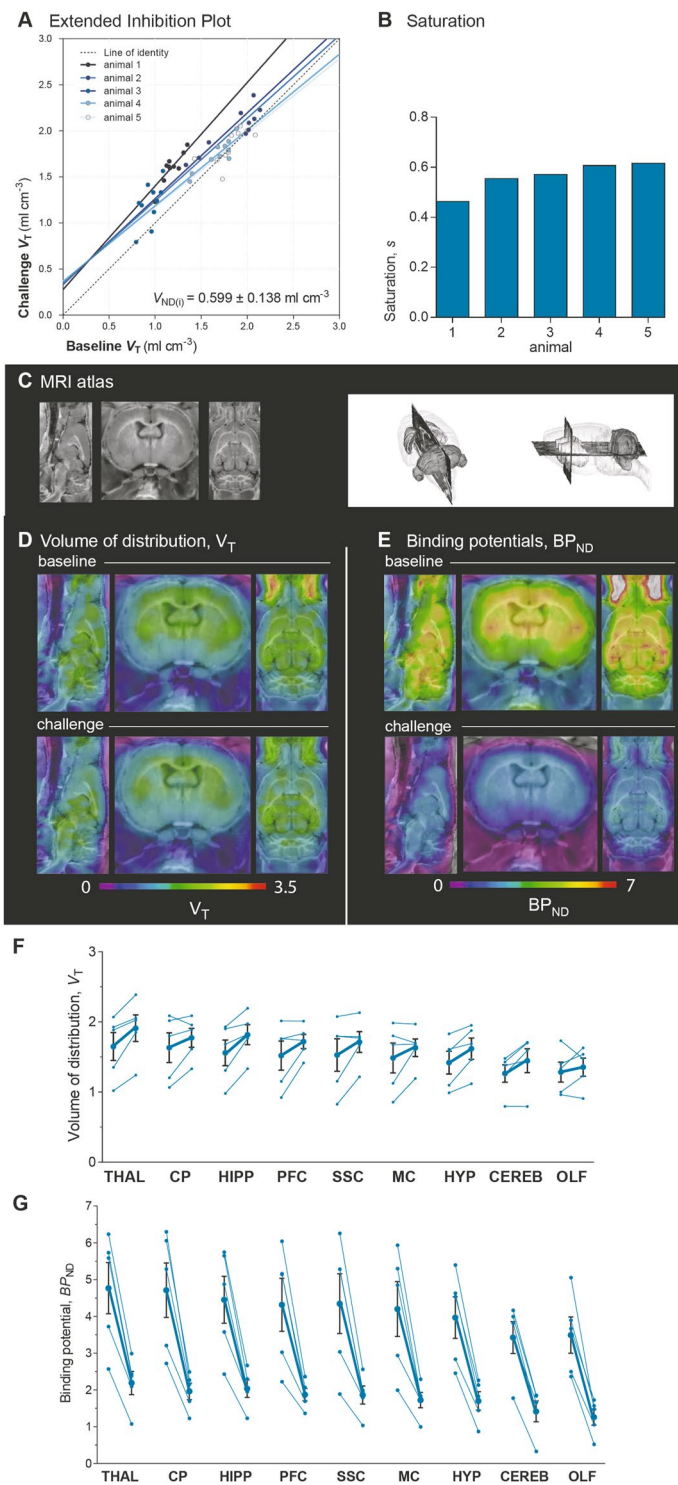
Figure 3. Extended Inhibition Plot. Due to significantly increased f_P in response to challenge, the Extended Inhibition Plot (eq. 36) (**A**) was applied to solve $V_{ND(i)}$. In the Extended Inhibition Plot, regional estimates of V_T at challenge condition are plotted versus the estimates at baseline. $V_{ND(b)}$ was set to 0.286 ml cm^{-3}, because this value was previously assessed in an identical strain of rats[16]. The solid lines illustrate the regression in individual animals and the stippled line illustrates the line of identity. The plots were constrained to produce one population-wise $V_{ND(i)}$ value, which yielded 0.599 ml cm^{-3}. The saturation, *s*, obtained by the Extended Inhibition Plot is presented for individual animals in (**B**). This revealed that 0.3 mg/kg yohimbine challenge blocked in average 56% of the available receptors. Panel (C) shows the MRI atlas, which the parametric images were superimposed on. Parametric images of V_T in panel (D) show that yohimbine challenge did not change [^{11}C]yohimbine V_T compared to baseline due to a masked effect. The real inhibition effect of yohimbine challenge was revealed when BP_{ND} was calculated using $V_{ND(i)}$ at 0.599 ml cm^{-3} (panel (E)). Correspondingly, the quantification of V_T and BP_{ND} at steady-state in panels (F,G) are consistent with the parametric maps. The

thin lines in (F) connect V_T at baseline and challenge in the same animal, and the thick line shows the average of the population. V_T was increased upon challenge with unlabelled yohimbine. The calculation of the BP_{ND} in (G) revealed a significant inhibition effect in response to challenge with unlabelled yohimbine (****$P < 0.0001$). The regional estimates of V_T and BP_{ND} are listed for individual animals in Table 1. THAL thalamus, CP caudate putamen, HIPP hippocampus, PFC prefrontal cortex, SSC somatosensory cortex, MC motor cortex, HYP hypothalamus, CEREB cerebellum, OLF olfactory bulb.

. . . .

widespread expression of α_2 adrenoceptors in the periphery may be another contributor to elevation of f_P by displacement of radioligand from sites in heart, pancreas[27], smooth muscles in blood vessels[28,29], kidneys[30], and platelets[31].

Elevated f_P may have influenced the findings by Jakobsen and colleagues[14] of a lack of dose-dependent reduction of labeled yohimbine accumulation with unlabeled yohimbine challenge in pigs. Competition with a low dose (0.07 mg/kg) yohimbine reduced the value of V_T of [^{11}C]yohimbine in porcine brain by approximately 30%. However, pre-treatment with a 24-fold higher dose (1.7 mg/kg) failed to decrease V_T further. Another selective ligand of α_2 adrenoceptors, RX821002, was used to challenge [^{11}C]yohimbine binding in porcine brain, where the low dose of 0.15 mg/kg caused greater decline of the value of V_T than the higher dose of 0.7 mg/kg. Although values of f_P were not determined in the study by Jakobsen and colleagues[14], increase of the value of f_P is a likely explanation, evident from findings *in vitro* that binding of yohimbine engages in dose-dependent competition with tritium-labeled yohimbine[32] and with RX821002[33].

In similar experiments by Smith *et al.*[34], [^{11}C]mirtazepin binding in porcine brain was sensitive to yohimbine competition in a dose-dependent manner, where challenge with 0.3 and 3.0 mg/kg yohimbine reduced [^{11}C]mirtazepin binding by 23% and 43%, respectively. In contrast, challenge with RX821002 at dose of 0.1 mg/kg reduced [^{11}C]mirtazepin binding by 35%, while a dose of 1 mg/kg failed to inhibit the binding further. It is unknown if the RX821002 challenge displaced plasma protein binding, but it is likely that RX821002 displaces binding to α_2 adrenoceptor sites in peripheral organs that potentially contributes to a higher value of f_P.

Pharmacological challenge by means of PET is a common test of the reversibility of radioligand binding. However, a number of studies have reported unaltered or increased occupancy of receptors after pharmacological challenge: A study of baboon brains showed that occupancy of 5-HT$_{2A}$ receptors by [^{18}F]altanserin, administered as constant infusion, was unaltered in the presence of extracellular levels of serotonin, elevated with fenfluramine, a selective serotonin reuptake inhibitor[35]. The binding of [^{18}F]altanserin is known to be sensitive to challenge with the 5-HT$_{2A}$ receptor antagonist, SR 46349 in baboons[35] and also to non-radiolabeled altanserin in rodent brain[36]. Similarly, a PET study of neuroinflammation revealed increased [^{11}C] PBR28 binding to the translocator protein (TSPO) in baboon brain in response to i.v. injection of 0.1 mg/kg LPS (lipopolysaccharide)[37]. The increases of binding at 1 and 4 hours post-administration were accompanied by increase of pro-inflammatory cytokines, causing the authors to propose that systemic inflammation by LPS can lead to increased TPSO expression. However, studies with infrared spectroscopy have shown that LPS binds to plasma albumin with the ratio 10:1, which changed the secondary structure of albumin[38]. Therefore, it cannot be excluded that increased [^{11}C] PBR28 binding after LPS administration is confounded by increase of f_P due to structural changes of albumin exerted by LPS. This possibility was confirmed recently by Hilmer *et al.*[39] who showed that a low dose of LPS (0.1 ng/kg) administered i.v. to rhesus macaque monkeys increased [^{11}C] PBR28 f_P by 38%, as V_T increased by 39%. Increased f_P was also found to be elevated in response to pharmacological challenge in a study of α_7 nicotinic acetylcholine receptors with [^{18}F] DBT-10[40], where the challenge with a dose of the antagonist ASEM at 1.24 mg/kg produced a two-fold increase of f_P. The authors quantified V_T/f_P as an outcome parameter in order to determine the net effect of pharmacological blocking. Taken together, the examples illustrate that changes of f_P are held to occur commonly in PET studies and knowledge of changes of f_P will be necessary to determine the true effect of pharmacological challenge. Therefore, lack of inhibition or evidence of increased binding in future studies must raise the concern of changes to f_P, measured with plasma ultrafiltration or equilibrium dialysis.

The direct relationship between increased f_P and masked effects of challenge on V_T must be interpreted with caution when f_P and V_T are determined in separate groups of animals, as in the present study. Another limitation of the Extended Inhibition Plot is the source of the baseline value of V_{ND} (estimated in a condition where f_P remains constant). Ideally, estimation of two V_{ND} values requires at least three PET acquisitions. Instead, it may be possible to use a population-based value of $V_{ND(b)}$ to estimate $V_{ND(i)}$, as demonstrated in the present study. This approach requires homogeneity of the study populations, with the added limitation that biological variability affects the accuracy of the V_{ND} estimates. We note that the value of f_P determined by plasma ultrafiltration is a steady-state estimate, whereas the exchange *in vivo* is a dynamic process, as discussed above, making it difficult to numerically extrapolate changes in f_P to changes in V_T. We suggest that f_P should be quantified solely to determine whether criteria are met to employ the original plot, without the extension. If there is significant change of the magnitude of f_P, the criteria may be met for the application of the Extended version of Inhibition Plot. As the plot operates with steady-state variables, the dynamic origin of f_P will not influence the outcome.

The findings of the present study show that the α_2 adrenoceptors are distributed throughout the brain. Regions with the greatest B_{max} estimates included thalamus, hippocampus, and caudate-putamen, where the densities ranged between 2.4 and 2.5 pmol/cm^3. The receptor density of caudate-putamen at 2.2 pmol/cm^3 (corresponds to 220 fmol/mg protein) agrees with *in vitro* receptor binding results from rat caudate-putamen with [^{3}H]rauwolscine, a stereoisomer of yohimbine that yielded an estimate of 197 fmol/mg protein[41].

To enable comparison with other studies, we converted the values of B_{max} per unit wet weight to values per unit dry weight of protein. Assuming that brain tissue contains 10% protein and dry weight therefore is one tenth of wet weight[42], the range of values of B_{max} in prefrontal cortex in this study is 216 fmol/mg protein, and the value

	Volumes of Distribution, V_T														
A	**rat 1**			**rat 2**			**rat 3**			**rat 4**			**rat 5**		
VOI	**BASE**	**COLD**	**(%)**	**BASE**	**COLD**	**(%)**	**BASE**	**COLD**	**(%)**	**BASE**	**COLD**	**(%)**	**BASE**	**COLD**	**(%)**
THAL	1.02	1.24	(22)	2.07	2.39	(15)	1.35	1.85	(37)	1.93	2.05	(7)	1.88	2.02	(7)
CP	1.06	1.33	(25)	2.02	2.09	(3)	1.20	1.61	(34)	2.09	1.96	(−6)	1.80	1.89	(5)
HIPP	0.98	1.33	(36)	1.93	2.19	(14)	1.31	1.76	(35)	1.90	1.97	(4)	1.68	1.82	(9)
PFC	0.92	1.41	(53)	2.01	2.01	(0)	1.15	1.61	(40)	1.76	1.74	(−1)	1.76	1.84	(4)
SSC	0.83	1.22	(47)	2.08	2.13	(3)	1.15	1.67	(45)	1.80	1.77	(−2)	1.80	1.79	(0)
MC	0.85	1.19	(39)	1.98	1.97	(−1)	1.12	1.62	(44)	1.67	1.68	(1)	1.80	1.70	(−6)
HYP	0.99	1.12	(13)	1.58	1.88	(18)	1.10	1.46	(33)	1.83	1.95	(7)	1.61	1.69	(5)
CEREB	0.79	0.79	(0)	1.48	1.71	(16)	1.26	1.59	(27)	1.43	1.70	(19)	1.38	1.45	(5)
OLF	0.96	0.91	(−6)	1.33	1.63	(22)	1.00	1.23	(23)	1.73	1.48	(−15)	1.40	1.54	(10)
B	**Binding potentials, BP_{ND}**														
	rat 1			**rat 2**			**rat 3**			**rat 4**			**rat 5**		
VOI	**BASE**	**COLD**	**(%)**	**BASE**	**COLD**	**(%)**	**BASE**	**COLD**	**(%)**	**BASE**	**COLD**	**(%)**	**BASE**	**COLD**	**(%)**
THAL	2.57	1.07	(−58)	6.23	2.99	(−52)	3.72	2.09	(−44)	5.73	2.43	(−58)	5.59	2.38	(−57)
CP	2.72	1.22	(−55)	6.06	2.49	(−59)	3.20	1.69	(−47)	6.30	2.26	(−64)	5.28	2.15	(−59)
HIP	2.43	1.22	(−50)	5.75	2.66	(−54)	3.57	1.95	(−46)	5.65	2.30	(−59)	4.87	2.05	(−58)
PFC	2.22	1.36	(−39)	6.04	2.36	(−61)	3.02	1.69	(−44)	5.16	1.90	(−63)	5.14	2.06	(−60)
SSC	1.88	1.03	(−45)	6.26	2.56	(−59)	3.03	1.79	(−41)	5.28	1.95	(−63)	5.28	1.99	(−62)
MC	1.99	0.99	(−50)	5.94	2.29	(−61)	2.93	1.71	(−42)	4.85	1.81	(−63)	5.30	1.84	(−65)
HYP	2.45	0.87	(−65)	4.53	2.13	(−53)	2.83	1.44	(−49)	5.40	2.26	(−58)	4.63	1.82	(−61)
CEREB	1.77	0.32	(−82)	4.16	1.85	(−56)	3.39	1.66	(−51)	3.99	1.84	(−54)	3.81	1.42	(−63)
OLF	2.36	0.51	(−78)	3.67	1.72	(−53)	2.50	1.05	(−58)	5.05	1.46	(−71)	3.90	1.57	(−60)

Table 1. Volumes of Distribution and Binding Potentials. The magnitude of V_T (**A**) at challenge increased significantly compared to baseline (*P < 0.05). The correct $V_{ND(i)}$ estimate obtained with the Extended Inhibition Plot was used to calculate BP_{ND} (**B**). This revealed the real inhibition effect of yohimbine challenge with 50–60% decline of BP_{ND} in the challenge condition compared to baseline (***P < 0.0001). VOI volume of interest, BASE baseline, COLD challenge with unlabeled yohimbine, % percent-wise change. THAL thalamus, CP caudate putamen, HIPP hippocampus, PFC prefrontal cortex, SSC somatosensory cortex, MC motor cortex, HYP hypothalamus, CEREB cerebellum, OLF olfactory bulb.

of K_D is 0.5 nM. To compare, we listed values of B_{max} and K_D from cortical areas of rat brain in Table 4. The table shows that comparison with results of *in vitro* binding assays is not simple, because of the great variability of findings of B_{max} and K_D among *in vitro* studies, depending on the method used.

The values of B_{max} in prefrontal cortex in the present study are closest to the result of [³H]yohimbine binding assays by Rout *et al.*[32] at 260 fmol/mg protein in the condition of no added magnesium in the assay. The authors demonstrated that [³H]yohimbine binding depends on many physiological factors such as pH, temperature, and Mg^{2+} concentration. We argue that the estimate by Rout *et al.*[32] in absence of Mg^{2+} is closer to the physiological condition and therefore more directly comparable to the present results than the condition with 10 mM Mg^{2+} present, considering the physiological level of Mg^{2+} in brain tissue of 230 μM[43]. While the B_{max} values are in range, the estimates of K_D are 20-fold higher than the present estimates. The discrepant values of K_D may relate to the method used to block non-specific binding. In the present study, the non-specific binding is computed as reflected in the value of V_{ND}, while the concentrations of competitors delivered to the binding sites *in vitro* often are in doubt because of the non-physiological delivery necessitated by the *in vitro* condition. Rout and colleagues used 100 μM noradrenaline to block non-specific binding, which may lead to an overestimation of K_D because noradrenaline and [³H]yohimbine compete at the specific binding sites of α_2 adrenoceptor.

In comparison to the results from [³H]yohimbine membrane binding studies by Brown *et al.*[44,45], values of B_{max} in the present study are 1.5-fold higher, while values of K_D are 10-fold lower. The variability of estimates of B_{max} and K_D therefore may be attributed by differences in the methods of blocking neccesary to determine non-specific binding. Brown and colleagues used 10 μM phentolamine that is known to antagonize α_1 and α_2 adrenoceptors with higher selectivity to α_1 adrenoceptor[46]. Thus, due to the affinity to α_1 and α_2 adrenoceptor, use of phentolamine may underestimate values of B_{max} and overestimate values of K_D, as α_1 and some α_2 adrenergic sites both may be blocked. The same blocking method was applied in the study by Boyajian *et al.*[41] to block [³H]RX821002 binding to α_2 adrenoceptor, the results of which are in agreement with the findings of Ribas and colleagues[7] with estimates of [³H]RX821002 B_{max} and K_D in the same range. Estimates of B_{max} generally are higher when determined with [¹¹C]yohimbine than with [³H]RX821002, possibly due to differential affinities to α_2 adrenoceptor subtypes. Yohimbine does not distinguish between the subtypes, whereas RX8201002 has a higher affinity to α_{2A} and α_{2C} than to α_{2B}[33]. Therefore, use of RX8201002 may underestimate the desnity of α_2 adrenoceptor sites. Altogether, more *in vivo* studies are essential to examine α_2 adrenoceptors in health and disease when physiological variables strongly influence α_2 adrenoceptor binding and are difficult to reproduce *in vitro*.
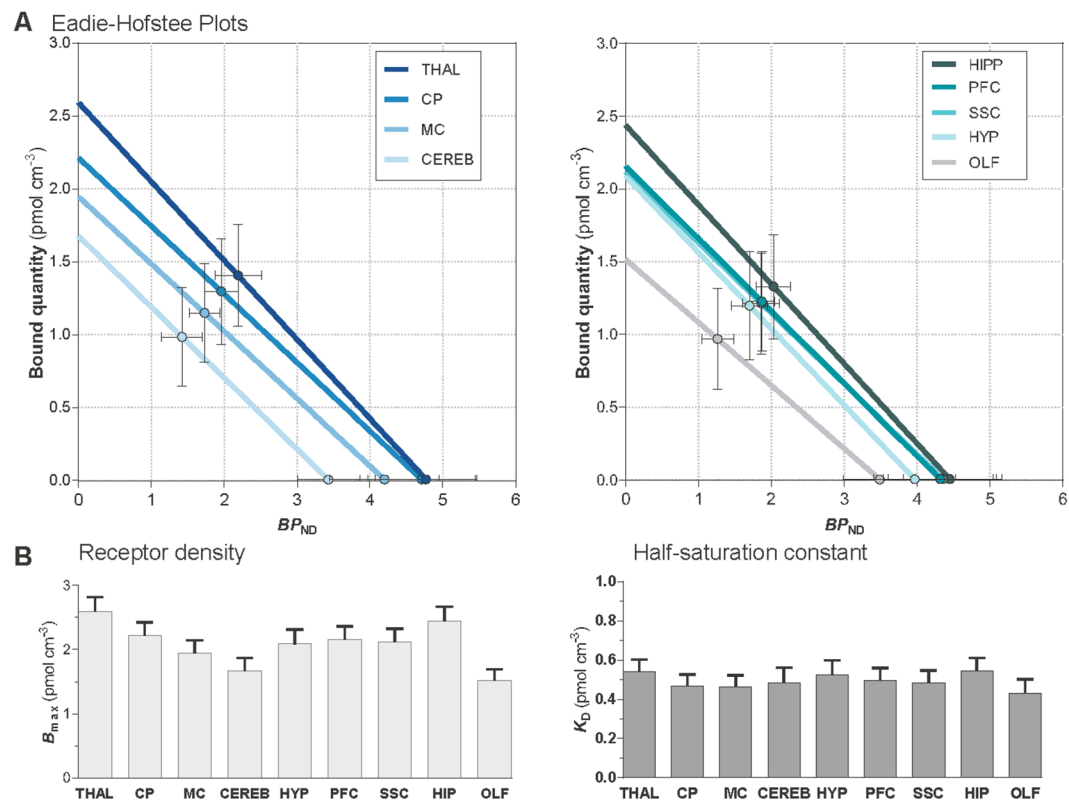
Figure 4. Eadie-Hofstee Plot. Eadie-Hofstee Plot (eq. 1 in Methods) presented in (**A**) solves the receptor density (B_{max}) and affinity ($1/K_D$) from a linear relationship between the bound quantity and binding potentials. The bound quantity was calculated using specific activity and BP_{ND} (eq. 2 in Methods). Receptor densities was obtained from the Y-intercept and the half-saturation constant, K_D, as the slope. Each bar represents the mean, the error bars correspond to the S.E.M. The highest densities of α_2 adrenoceptors were found in thalamus, hippocampus, caudate putamen and prefrontal cortex, whereas lowest densities were found in cerebellum and olfactory bulb ((**B**) left). K_D was at a similiar level in all examined regions at approximately 0.5 mM ((**B**) right) The regional receptor densities and K_D are also listed in Table 2, and the specific activities that were used for calculation of bound quantity are listed in detail in Table 3. THAL thalamus, CP caudate putamen, HIPP hippocampus, PFC prefrontal cortex, SSC somatosensory cortex, MC motor cortex, HYP hypothalamus, CEREB cerebellum, OLF olfactory bulb.

	B_{max} (pmol cm^{-3}) mean ± S.E.M.	K_D (nM) mean ± S.E.M.
THAL	2.59 ± 0.50	0.54 ± 0.14
CP	2.21 ± 0.48	0.47 ± 0.13
HIPP	2.44 ± 0.51	0.55 ± 0.15
PFC	2.16 ± 0.46	0.50 ± 0.14
SSC	2.12 ± 0.47	0.48 ± 0.14
HYPP	2.09 ± 0.50	0.52 ± 0.16
MC	1.95 ± 0.44	0.46 ± 0.14
CEREB	1.68 ± 0.45	0.49 ± 0.17
OLF	1.52 ± 0.41	0.43 ± 0.16

Table 2. Receptor Density and Half-Saturation Constant. The receptor density (B_{max}) and affinity ($1/K_D$), solved from Eadie-Hofstee plot (shown in Fig. 4A), are listed here for individual animals. This demonstrates that areas with densely expressed α_2 adrenoceptors include thalamus, hippocampus, caudate putamen, and prefrontal cortex, whereas cerebellum and olfactory bulb were regions with lower density. Interestingly, K_D was higher in regions with enriched α_2 adrenoceptors and low in regions with low density, supporting that receptor affinity is greater in areas with low receptor expression.

We estimated values of B_{max} and K_D with the Eadie-Hofstee plot from only two magnitudes of receptor occupancy, which may lower the accuracy. Ideally, more levels of occupancy yield more accurate regressions. However, due to the limited blood volume in rats, we did not perform additional PET acquisitions that would result in greater loss of blood that in turn would initiate compensatory physiological changes (increased heart rate and vasoconstriction) that affect

	Radioactivity (MBq)		Total quantity (pmol)		Specific activity (kBq pmol^{-1})	
	BASE	COLD	BASE	COLD	BASE	COLD
rat 1	16.2	20.5	0.164	243	98988	84
rat 2	21.5	25.5	4.374	242	4916	106
rat 3	30.7	31.1	0.847	224	36267	139
rat 4	30.2	39.1	0.564	234	53514	167
rat 5	27.4	32.6	0.049	240	554889	136
mean	25.35	28.6	1.019	235	161910	122

Table 3. Specific Activity. The specific activity was used to quantify the bound quantity from eq. 2. The table shows the injected radioactivity, total quantity of unlabeled yohimbine and specific activity for individual animals at baseline and challenge condition. BASE baseline, COLD challenge with unlabeled yohimbine.

	Methods						Results		
Reference	Radioligand	pH	temp (°C)	mg^{2+}	Blocking of NS		Brain area	B_{max} (fmol/mg protein)	K_D (nM)
This study	[^{11}C]yohimbine	*in vivo*, physiological condition			mathematical, 0.3 mg/kg YOH		prefrontal cortex	216	0.50
Rout et al.[32]	[^{3}H]yohimbine membrane assay	7.0	25.0	0 mM	noradrenaline 100 μM		cortex	260	9.86
		7.0	25.0	10 mM	noradrenaline 100 μM		cortex	157	11.06
Brown et al.[44]	[^{3}H]yohimbine membrane assay	7.4	25.0	0	phentolamine 10 μM		cerebral cortex	121	5.20
Brown et al.[45]	[^{3}H]yohimbine membrane assay	7.4	25.0	0	phentolamine 10 μM		cerebral cortex	121	5.30
Ribas et al.[7]	[^{3}H]RX821002 binding assay	7.5	25.0	1 mM	adrenaline 10 μM		parieto-occipital cortex	92.0	0.57
Ribas et al.[68]	[^{3}H]RX821002 binding assay	7.5	25.0	1 mM	adrenaline 10 μM		parieto-occipital cortex	81.0	0.50
Boyajian et al.[41]	[^{3}H] -rauwolscine autoradiography	7.7	22	0	phentolamine 10 μM		anterior forebrain	109	0.79

Table 4. Comparison of B_{max} and K_D estimates. The estimates from the present study was compared with previous data from *in vitro studies*. The data and experimental conditions are listed here.

radioligand delivery to the brain. The method presented here can be applied to larger mammals with greater blood volumes that enable estimates of B_{max} and K_D with higher accuracy. We acknowledge that receptor density and affinity estimated *in vivo* may not necessary reflect the ultimate estimates determined *in vitro*, because *in vivo* experiments often are performed in animals anesthetized with gas anesthetics known to elevate noradrenaline[47].

In conclusion, we demonstrated the use of the Extended Inhibition Plot to quantify the binding potentials of [^{11}C]yohimbine and density of α_2 adrenoceptors in the living brain with PET. The method enables the analysis of future investigations of the noradrenergic and other transmission systems with wide distributions in brain, such as the nicotinic cholinergic system[48].

Methods
Novel Quantitative Analysis of Specific Binding to Brain Receptors.
We derived the present method from well-known principles of kinetics. We identified the following six steps to the determination of binding parameters of radioligands that achieve receptor occupancy. The binding parameters are constants in the fundamental equation that underlies the Eadie-Hofstee plot[49,50],

$$B = B_{max} - K_D BP_{ND} \tag{1}$$

where B_{max} is the maximum binding capacity and $1/K_D$ the affinity of the receptors. The variable B is the bound quantity of the ligand, and BP_{ND} is the binding potential of the radioligand at the specific degree of occupancy. To solve the equation of the Eadie-Hofstee plot for the two parameters, it is necessary to know the bound quantities of the ligand and the binding potentials in at least two conditions of different occupancy. The bound quantity is related to the binding potential by the relationship,

$$B = M \left(\frac{BP_{ND}}{1 + BP_{ND}} \right), \tag{2}$$

where M is the total mass of the ligand per unit volume of brain tissue, calculated from the known specific activity of the radioligand. The binding potential in turn is the ratio between the quantities of specifically (and hence displaceably) bound ligand and the unbound (and hence non-displaceable) ligand, equal to the ratio of the volumes of distribution of displaceable and non-displaceable ligand quantities,

$$BP_{ND} = \frac{V_T - V_{ND}}{V_{ND}}. \tag{3}$$

where V_T is the apparent volume of distribution of all tracer in the tissue, and V_{ND} is the apparent volume of distribution of unbound and hence non-displaceable tracer in the tissue, relative to the concentration in arterial plasma at steady-state.

Integral uptake equation. The first step is the kinetic analysis of tracer accumulation. The simplest mathematical description of the pharmacokinetic behavior of radiotracers in brain is the one-tissue compartment model (Fig. 1A) that assumes approach to a secular steady-state across the blood-brain barrier,

$$\frac{dm_1(t)}{dt} = V_0 \frac{dc_a(t)}{dt} \tag{4}$$

and

$$\frac{dm_2(t)}{dt} = K_1 c_a(t) - k_2' m_2(t), \tag{5}$$

where the total tracer quantities in the vascular system (both free and bound to plasma proteins), m_1, are distributed in the vascular volume, V_0, and $c_a(t)$ reflects the concentration in that volume. Although, m_1 reflects the total quantity of ligand in plasma, only the free amount is exchangable across the BBB (Fig. 1A).

The term m_2 refers to tracer in brain tissue that reflects the clearance K_1 from the circulation and the fractional clearance k_2' from the tissue. Linearized solutions yield the constants K_1 and k_2', as previously summarized by Nahimi *et al.*[12] and Phan *et al.*[16]. Briefly, at steady-state, V_T equals the ratio K_1/k_2' where K_1 is a function of blood flow, F, free plasma fraction, f_P, and the permeability- surface area of the vascular bed, PS,

$$K_1 = f_P F (1 - e^{-PS/(f_P F)}), \tag{6}$$

and k_2' is,

$$k_2' = \frac{k_2}{1 + BP_{ND}} = \frac{K_1}{V_{ND}(1 + BP_{ND})} \tag{7}$$

where k_2 is the rate of efflux from V_{ND}, and BP_{ND} is the binding potential. Therefore, at steady-state, the values of K_1 (eq. 6) and k_2' (eq. 7) yield,

$$k_2 = k_2'(1 + BP_{ND}) = \frac{K_1}{V_{ND}}. \tag{8}$$

At steady-state, the K_1/k_2' ratio defines the total volume of distribution in tissue (V_T) as determined by the total concentration in brain relative to plasma,

$$V_T = \frac{K_1}{k_2'} \tag{9}$$

Equations 4 and 5 together define the exchange of tracer in the brain tissue as a whole,

$$\frac{dm(t)}{dt} = \frac{dm_1(t)}{dt} + \frac{dm_2(t)}{dt} = V_0 \frac{dc_a(t)}{dt} + K_1 c_a(t) - k_2' m_2(t) \tag{10}$$

from which the total quantity of tracer, m, is the sum of the solutions to the differential equations,

$$m(T) = m_1(T) + m_2(T) = V_0 c_a(T) + K_1 \int_0^T c_a(t)\, dt - k_2' \int_0^T m_2(t)\, dt \tag{11}$$

As m_2, is unknown, eq. 11 is solved by substitution of the expression, $m(1 - m_1/m)$,

$$m(T) = V_0 c_a(T) + K_1 \int_0^T c_a(t)\, dt - k_2' \int_0^T m(t) \left(1 - \frac{m_1(t)}{m(t)}\right) dt \tag{12}$$

but when steady-state is approached, the m_1/m ratio becomes negligible and eq. 12 reduces to,

$$m(T) = K_1 \int_0^T c_a(t)\, dt - k_2' \int_0^T m(t)\, dt \tag{13}$$

Volumes of distribution from linearized graphical analysis of tracer kinetics. The second step is the choice of any one of several graphical solutions to eq. 13 based on dynamic measurements of any two of three kinetic variables that include the apparent volume of distribution, V_{app}, [ml cm^{-3}]

$$V_{\text{app}}(T) = \frac{\int_0^T m(t)\,dt}{\int_0^T c_a(t)\,dt},$$

(14)

the apparent clearance of radioligand from plasma to brain, K_{app}, [ml cm^{-3} min^{-1}],

$$K_{\text{app}}(T) = \frac{m(T)}{\int_0^T c_a(t)\,dt},$$

(15)

and the apparent residence time in the brain [min],

$$\Theta(T) = \frac{\int_0^T m(t)\,dt}{m(T)}.$$

(16)

Six linearizations previously derived to obtain estimates of K_1 and k_2' from steady-state solutions of eq. 13 used combinations of two out of the three dynamic variables (eqs 14, 15 and 16), including two regressions with negative slopes ('N1' and 'N2'), and four regressions with positive slopes ('P1-P4'). The 'N1' graph plotted the apparent clearance as a function of the apparent volume of distribution as derived by Gjedde *et al.*[51] and Cumming *et al.*[52] by dividing eq. 13 by $\int_0^T c_a(t)dt$,

$$\textbf{N1} \quad K_{\text{app}}(T) = K_1 - k_2'\,V_{\text{app}}(T),$$

(17)

where K_1 and k_2' represent y-intercept and slope, respectively. The 'N2' plot was derived by Gjedde *et al.*[53] as the mirror of 'N1',

$$\textbf{N2} \quad V_{\text{app}}(T) = V_T - \frac{1}{k_2'}K_{\text{app}}(T),$$

(18)

where V_T is the y-intercept and k_2' is the reciprocal value of the slope. Division of eq. 13 by $m(T)$ and k_2' yields the 'P1' plot with a positive slope of the linear relationship between the reciprocal value of $K_{\text{app}}(T)$ and $\Theta(T)$[51],

$$\textbf{P1} \quad \frac{1}{K_{\text{app}}(T)} = \frac{1}{V_T}\Theta(T) + \frac{1}{K_1},$$

(19)

where V_T is the reciprocal value of the slope, and K_1 is the reciprocal value of the y-intercept. Logan and colleagues[54] derived the 'P2' plot as the mirror of 'P1',

$$\textbf{P2} \quad \Theta(T) = V_T\frac{1}{K_{\text{app}}(T)} - \frac{1}{k_2'},$$

(20)

where V_T is the slope of the line. The 'P3' plot was introduced by Reith *et al.*[55] by division of eq. 13 with $\int_0^T m(t)\,dt$,

$$\textbf{P3} \quad \frac{1}{\Theta(T)} = K_1\frac{1}{V_{\text{app}}(T)} - k_2',$$

(21)

where K_1 is the slope and k_2' the y-intercept. Nahimi *et al.*[12] described the mirror version, 'P4',

$$\textbf{P4} \quad \frac{1}{V_{\text{app}}(T)} = \frac{1}{K_1}\frac{1}{\Theta(T)} + \frac{1}{V_T}$$

(22)

where K_1 is the reciprocal of the slope and V_T is the reciprocal of the y-intercept. All six plots yielded similar estimates of K_1, k_2', and V_T when the parameters were estimated in the same time frames at steady-state. We applied all six plots because they have different sensitivities to linearity. We note that the Logan plot ('P2') and it's mirror version, 'P1' plot, readily but deceptively approached linear relationships that remained linear throughout acquisition time, whereas the alternative plots ('N1', 'N2', 'P3', 'P4') lost linearity when steady-state was disrupted (Supplemental Fig. S2). Because the value of V_T strictly is defined only at steady-state and because the later analysis steps are sensitive to the accuracy of values of V_T, we applied all six plots to know when steady-state is present. The time frames of steady-state were objectively chosen based on the goodness of fit from iterative analysis (as described in details in Data Analysis).

Reference Volume of Distribution from Inhibition Plots. The third step is to estimate the volume of distribution of non-displaceable tracer, V_{ND}, most simply from a brain region with no specific binding of the ligand. If no such region exists, V_{ND} can be estimated by pharmacological blocking of specific binding, graphically solved with one of three plots, the so-called Inhibition, Saturation, and Occupancy plots. The Saturation Plot was first derived by Lassen and colleagues[56],

$$V_{T(b)} = \frac{1}{s} \Delta V_T + V_{ND},$$ (23)

where ΔV_T, the difference of distribution volumes between baseline and response to pharmacological challenge, is plotted as a function of the volume of distribution at baseline, $V_{T(b)}$. The symbol s denotes the degree of saturation as the fraction of occupied receptors, and V_{ND} is the estimate of the y-intercept. Cunningham *et al.*[57] derived the Occupancy Plot as the mirror of the Saturation plot,

$$\Delta V_T = s\,V_{T(b)} - s\,V_{ND}.$$ (24)

while the Inhibition Plot previously was introduced by Gjedde and Wong[58] and Gjedde *et al.*[53], with the distribution volume in the challenge condition $V_{T(i)}$ plotted directly as a function of $V_{T(b)}$,

$$V_{T(i)} = (1 - s)\,V_{T(b)} + s\,V_{ND},$$ (25)

where V_{ND} is the intercept of the Inhibition Plot with the line of identity.

The three plots were derived from a common expression of the relative receptor availability at inhibition, $BP_{ND(i)}$, and baseline, $BP_{ND(b)}$,

$$1 - s = \frac{BP_{ND(i)}}{BP_{ND(b)}},$$ (26)

where $1 - s$ denotes the fraction of available receptors in the presence of a competitor. The BP_{ND} equals,

$$BP_{ND(i)} = \frac{V_{T(i)} - V_{ND(i)}}{V_{ND(i)}},$$ (27)

and

$$BP_{ND(b)} = \frac{V_{T(b)} - V_{ND(b)}}{V_{ND(b)}},$$ (28)

where $V_{ND(i)}$ and $V_{ND(b)}$ denote the distribution volumes of non-displaceable tracer at inhibition and baseline, respectively. When the volumes are constant at the two conditions, ($V_{ND(i)} = V_{ND(b)} = V_{ND}$), eqs 26, 27 and 28 yield the expression of relative receptor availability in terms of volumes of distribution,

$$1 - s = \frac{V_{T(i)} - V_{ND}}{V_{T(b)} - V_{ND}},$$ (29)

where rearrangement of eq. 29 yields the Inhibition Plot (eq. 25), Saturation (eq. 23), and Occupancy (eq. 24) plots.

A requirement of application of any plot is that f_P, the free fraction of radioligand in plasma, must remain unchanged at baseline and challenge. At steady-state, the V_{ND} value is the ratio of the total concentrations of radioligand in blood, C_a, and brain, C_{ND},

$$V_{ND} = V_D \frac{C_{ND}}{C_a}$$ (30)

where V_D is the volume in which C_{ND} is the concentration. The concentrations C_a and C_{ND} also are the concentrations of freely dissolved ligands in plasma C_{FP} and tissue water, C_{FT},

$$C_{FP} = f_P\,C_a,$$ (31)

and

$$C_{FT} = f_{FT}\,C_{ND}.$$ (32)

such that the combination of eqs 30, 31 and 32 yields,

$$V_{ND} = V_D \frac{f_P}{f_{ND}} \frac{C_{FT}}{C_{FP}}$$ (33)

where V_{ND} is a product of a physical volume, V_D, and two unitless ratios. The f_P to f_{ND} ratio depends on the non-specific binding in plasma and brain tissue, while the C_{FT} to C_{FP} ratio depends on properties of the blood-brain barrier (BBB). Assuming that the radioligand enters the brain tissue by passive diffusion, and free concentrations at steady-state the of ligand across BBB are equal, eq. 33 reduces to,

$$V_{ND} = V_D \frac{f_P}{f_{ND}}.$$ (34)

such that a rise of f_P would change the magnitude of V_{ND}.

Variable reference volumes of distribution from Extended Inhibition Plot. The fourth step is the correction for a change of the reference volume of distribution when plasma free fractions, f_P, have changed in response to pharmacolgcial challenge. In this case, eq. 29 can be applied in its unreduced form,

$$1 - s = \left(\frac{V_{T(i)} - V_{ND(i)}}{V_{T(b)} - V_{ND(b)}}\right)\left[\frac{V_{ND(b)}}{V_{ND(i)}}\right], \tag{35}$$

where $V_{ND(b)}$ and $V_{ND(i)}$ are the magnitudes at baseline and at inhibition. Isolation of $V_{T(i)}$ in eq. 35 yields the Extended Inhibition Plot,

$$V_{T(i)} = (1 - s)\left[\frac{V_{ND(i)}}{V_{ND(b)}}\right]V_{T(b)} + s\,V_{ND(i)}, \tag{36}$$

takes the changes of f_P and V_{ND} into account. The value of $V_{ND(b)}$ must be known to solve for $V_{ND(i)}$ in eq. 36, for example with reference to a pharmacological challenge that affects the receptor binding without altering f_P, by modulating the release or depletion of endogenous transmitter. In contrast, challenge with a unlabeled ligand may raise f_P, when the challenge with unlabeled ligand displaces ligand bound to plasma proteins. Challenge with unlabeled yohimbine may reduce the protein binding of the radioligand when as much as 82% of labeled yohimbine is bound to plasma proteins[22].

Calculation of binding potentials from total and reference volumes. The fifth step is the calculation of binding potentials from volumes of distribution. The binding potential, BP_{ND}, is the ratio of specifically bound to non-displaceable ligand quantities in the tissue[20,21]. The BP_{ND} is determined from the total volume of distribution in the tissue, V_T, and the volume of distribution of non-displaceable ligand, V_{ND}, determined at the respective conditions of variable occupancy,

$$BP_{ND} = \frac{V_T - V_{ND}}{V_{ND}}. \tag{37}$$

where V_{ND} is obtained from a reference region devoid of specific receptors. In the case of yohimbine, α_2 adrenoceptors are widely distributed in the brain, with no suitable reference region.

Determination of B_{max} and K_D estimates from Eadie-Hofstee Plot. The sixth and final step was the graphical solution to the Eadie-Hofstee Plot of eq. (1) (Eadie 1952, Hofstee 1952), where B is the bound quantity and BP_{ND} is the binding potential of ligands. We calculated the bound quantity from the relationship described by eq. 2.

Animals. Animal experiments were conducted according to the protocol approved by the Danish Animal Experiments Inspectorate in compliance with the law regulated by the Danish Ministry of Food, Agriculture and Fisheries. Five female Sprague Dawley rats (weighing 250–300 g) were housed two per cage with access to food and water ad libitum under 12/12 hours light/dark cycle conditions. The animals had two consecutive 90-minute PET acquisitions on the same day. Anesthesia was induced in a chamber with 5% isoflurane, maintained by mask with 2% isoflurane until the end of PET recording. To raise the delivery of yohimbine to the brain by limiting the reaction of yohimbine with p-glycoprotein at the BBB[59], we gave animals cyclosporine i.v. 50 mg/kg 30 minutes before the baseline PET. With a half-life longer than 10 hours at doses exceeding 30 mg/kg[60], only one dose was needed. We administered unlabeled yohimbine 5–10 min before the second acquisition at an IV dose of 0.3 mg/kg.

PET acquisitions and image processing. Animals were imaged in a tomograph designed for rodents (microPET R4, CTI Concorde Microsystems, Knoxville, TN, USA), with a spatial resolution at the center of the field of view at 3.69 mm³ [61]. PET images were processed with MINC software of McConnell Brain Imaging Centre, Montreal Neurological Institute, McGill University. We reconstructed the photon attenuation correction of dynamic recordings by 3D-filtered back projection, resulting in a $128 \times 128 \times 63$ matrix. Summed emission recordings were coregistered to a digital MRI atlas of the rat brain, using the program Register of MINC software. The dynamic emission recordings were resampled to the same 3D-space of the MRI rat brain atlas. We used masks of volumes of interest (VOIs) developed by Schiffer *et al.*[62], which we resampled to MRI space. The masks were then used to extract time-activity curves from the resampled dynamic data sets.

Data analysis. We developed the user-friendly, open-source graphical user interface Kinetic Windows (KiWi) in MATLAB to aid robust and effective kinetic analysis. KiWi enables users to import time-activity curves, to plot dynamic PET parameters as functions of time (eqs 14–16), and ultimately to simultaneously plot data with the N1–N2 or P1–P4 plots. The uptake phase with the optimal dynamic data fit is objectively chosen in KiWi, identified as the frames with the r-squared precision closest to unity. The software is available on Github[63] and MATLAB file exchange[64]. Time-activity curves for each region were analyzed together with the corresponding plasma activity curve as input. Here, we chose estimates of V_T obtained graphically from N2 plot (eq. 18) derived by Gjedde *et al.*[53]. Parametric maps of BP_{ND} were constructed by means of eqs 27 and 28.

Plasma Ultrafiltration. To test the change of f_P incurred by unlabeled yohimbine challenge relative to baseline, plasma ultrafiltration was performed as previously described by Gandelman *et al.*[65] and plasma free fractions quantified both *ex vivo* and *in vitro* (the method is illustrated in Fig. 2D left). In the *ex vivo* experiment, a separate group of six female Sprague Dawley rats were subjected to plasma ultrafiltration and treated identically to animals

that underwent PET acquisition. We administered cyclosporine (50 mg/kg) i.v., and we sampled arterial blood by catheter in the femoral artery. Samples from the baseline condition were collected 30 min after the cyclosporine treatment. To obtain blood from the unlabeled ligand challenge condition, we administered unlabeled yohimbine (0.3 mg/kg i.v.) and collected blood samples after 30 min. We centrifuged the blood samples in heparinized tubes for 20 min at 4 °C to generate plasma and stored the samples at −50 °C.

In the *in vitro* experiments, blood was drawn and yohimbine or amphetamine were added to the plasma samples later. The amounts of yohimbine and amphetamine added to the samples were calculated from the linear relationship between blood volume and body weight in rats[66]. The calculation assumed that plasma comprises 50% of the blood volume in rats and that the drug initially is distributed throughout plasma. The calculated amounts of drug were added to individual plasma samples. Thus 5 μg corresponded to a low yohimbine dose of 0.3 mg/kg and 25 μg to a higher dose of 1.5 mg/kg.

To measure f_P, we used the Centrifree centrifugal filter device (Millipore, Bedford, MA) with a molecular cutoff of 30 kDa for all samples. This pore size was chosen to ensure filtration of the yohimbine fraction bound to albumin with a molecular weight of approximately 65 kD in rats[67]. On the day of f_P determination, the plasma samples were thawed in room temperature in 20 min. Each sample unit of 1000 μl plasma was spiked with 50 μl [^{11}C]yohimbine. After 10 minutes incubation at room temperature, aliquots of 50 μl of this solution were used to measure the total activity (unfiltered plasma). For triplicate measurements of the filtered plasma, the remaining volume was divided into three ultrafiltration devices and centrifuged for 20 min using a centrifuge with a fixed angle rotor at 1000 g. After filtration, we removed aliquots of 50 μl to assess the activity in protein-free plasma. The activity of filtered plasma was determined in triplicates. All samples were counted in a gamma device (Packard Cobra Gamma Counter, Model D5003). Non-specific binding of the tracer to the ultrafiltration device was recovered by performing the same procedure on a phosphate-buffered solution. The correction factor, r, was determined as the ratio of the activity in the phosphate buffer before filtration, $A_{buffer(total)}$, to the filtered buffer, $A_{buffer(ultrafiltrate)}$,

$$r = \frac{A_{buffer(total)}}{A_{buffer(ultrafiltrate)}},$$
(38)

from which the plasma-free fraction, f_P, was calculated as the ratio of the activity of the filtered plasma, $A_{plasma(ultrafiltrate)}$, to the unfiltered plasma, $A_{plama(total)}$, multiplied by the correction factor, r, for recovery,

$$f_P = r \frac{A_{plasma(ultrafiltrate)}}{A_{plasma(total)}},$$
(39)

Statistics. To determine f_P elevation in response to unlabeled yohimbine challenge, we applied a non-parametric two-tailed test for the *ex vivo* assay. For the *in vitro* assay, we applied two-way ANOVA followed by Tukey's post-hoc analysis. To examine whether yohimbine challenge changed V_T and BP_{ND} compared to baseline, two-way ANOVA followed and Tukey's post-hoc analysis was applied. For all tests, a probability of less than 0.05 was considered significant. Statistical analyses were carried out in GraphPad Prism v7.

References
1. Braak, H. & Del Tredici, K. The pathological process underlying alzheimer's disease in individuals under thirty. *Acta neuropathologica* **121**, 171–181 (2011).
2. Sitte, H. H. *et al*. Dopamine and noradrenaline, but not serotonin, in the human claustrum are greatly reduced in patients with parkinson's disease: possible functional implications. *Eur. J. Neurosci.* **45**, 192–197 (2017).
3. Delgado, P. & Moreno, F. Antidepressants and the brain. *Int. Clin. Psychopharmacol.* **14**, S9–S16 (1999).
4. Gonzalez-Maeso, J., Rodriguez-Puertas, R., Meana, J., Garcia-Sevilla, J. & Guimon, J. Neurotransmitter receptor-mediated activation of g-proteins in brains of suicide victims with mood disorders: selective supersensitivity of [alpha] 2A-adrenoceptors. *Mol. psychiatry* **7**, 755 (2002).
5. Garca-Sevilla, J. A. *et al*. Up-regulation of immunolabeled α2A-adrenoceptors, gi coupling proteins, and regulatory receptor kinases in the prefrontal cortex of depressed suicides. *J. neurochemistry* **72**, 282–291 (1999).
6. Meana, J. J., Barturen, F. & Garcia-Sevilla, J. A. α2-adrenoceptors in the brain of suicide victims: increased receptor density associated with major depression. *Biol. psychiatry* **31**, 471–490 (1992).
7. Ribas, C., Miralles, A., Busquets, X. & Garca-Sevilla, J. A. Brain α2-adrenoceptors in monoamine-depleted rats: increased receptor density, g coupling proteins, receptor turnover and receptor mrna. *Br. journal pharmacology* **132**, 1467–1476 (2001).
8. Wiste, A. K., Arango, V., Ellis, S. P., Mann, J. J. & Underwood, M. D. Norepinephrine and serotonin imbalance in the locus coeruleus in bipolar disorder. *Bipolar disorders* **10**, 349–359 (2008).
9. Yatham, L. N. *et al*. A positron emission tomography study of norepinephrine transporter occupancy and its correlation with symptom response in depressed patients treated with quetiapine xr. *Int. J. Neuropsychopharmacol.* (2017).
10. Hesse, S. *et al*. The association between *in vivo* central noradrenaline transporter availability and trait impulsivity. *Psychiatry Res. Neuroimaging* **267**, 9–14 (2017).
11. Sara, S. J. & Bouret, S. Orienting and reorienting: the locus coeruleus mediates cognition through arousal. *Neuron* **76**, 130–141 (2012).
12. Nahimi, A. *et al*. Mapping α2 adrenoceptors of the human brain with ^{11}C-yohimbine. *J. Nucl. Medicine* **56**, 392–398 (2015).
13. Landau, A. M., Doudet, D. J. & Jakobsen, S. Amphetamine challenge decreases yohimbine binding to α2 adrenoceptors in landrace pig brain. *Psychopharmacol* **222**, 155–163 (2012).
14. Jakobsen, S. *et al*. Detection of α2-adrenergic receptors in brain of living pig with ^{11}C-yohimbine. *J. Nucl. Medicine* **47**, 2008–2015 (2006).
15. Thomsen, M. B. *et al*. Neonatal domoic acid alters *in vivo* binding of [^{11}C] yohimbine to α2-adrenoceptors in adult rat brain. *Psychopharmacol* **233**, 3779–3785 (2016).
16. Phan, J.-A. *et al*. Quantification of [^{11}C] yohimbine binding to α2 adrenoceptors in rat brain *in vivo*. *J. Cereb. Blood Flow & Metab* **35**, 501–511 (2015).

17. Landau, A. M. *et al*. Decreased *in vivo* α2 adrenoceptor binding in the flinders sensitive line rat model of depression. *Neuropharmacol* **91**, 97–102 (2015).

18. Muller, P. Y. & Milton, M. N. The determination and interpretation of the therapeutic index in drug development. Nat. reviews. *Drug discovery* **11**, 751 (2012).

19. Pisani, V. *et al*. Increased blood-cerebrospinal fluid transfer of albumin in advanced parkinson's disease. *J. neuroinflammation* **9**, 188 (2012).

20. Gjedde, A., Wong, D. F., Rosa-Neto, P. & Cumming, P. Mapping neuroreceptors at work: on the definition and interpretation of binding potentials after 20 years of progress. *Int. review neurobiology* **63**, 1–20 (2005).

21. Innis, R. B. *et al*. Consensus nomenclature for *in vivo* imaging of reversibly binding radioligands. *J. Cereb. Blood Flow & Metab.* **27**, 1533–1539 (2007).

22. Berlan, M., Verge, R. L., Galitzky, J. & Corre, P. L. α2-adrenoceptor antagonist potencies of two hydroxylated metabolites of yohimbine. *Br. journal pharmacology* **108**, 927–932 (1993).

23. Cameron, O. G., Zubieta, J. K., Grunhaus, L. & Minoshima, S. Effects of yohimbine on cerebral blood flow, symptoms, and physiological functions in humans. *Psychosom. Medicine* **62**, 549–559 (2000).

24. Zaretsky, D. V., Zaretskaia, M. V., DiMicco, J. A. & Rusyniak, D. E. Yohimbine is a 5-HT 1A agonist in rats in doses exceeding 1 mg/kg. *Neurosci. letters* **606**, 215–219 (2015).

25. Duong, T. Q. & Kim, S.-G. *In vivo* MR measurements of regional arterial and venous blood volume fractions in intact rat brain. *Magn. resonance medicine* **43**, 393–402 (2000).

26. Zucker, S. D., Goessling, W. & Gollan, J. L. Kinetics of bilirubin transfer between serum albumin and membrane vesicles insight into the mechanism of organic anion delivery to the hepatocyte plasma membrane. *J. Biol. Chem.* **270**, 1074–1081 (1995).

27. Saito, M., Saitoh, T. & Inoue, S. Alpha 2-adrenergic modulation of pancreatic glucagon secretion in rats. *Physiol. & behavior* **51**, 1165–1171 (1992).

28. MacMillan, L. B., Hein, L., Smith, M. S., Piascik, M. T. & Limbird, L. E. Central hypotensive effects of the alpha2a-adrenergic receptor subtype. *Science* **273**, 801 (1996).

29. Gavin, K., Colgan, M.-P., Moore, D., Shanik, G. & Docherty, J. α2C-adrenoceptors mediate contractile responses to noradrenaline in the human saphenous vein. *Naunyn-Schmiedeberg's archives of pharmacology* **355**, 406–411 (1997).

30. Hein, L., Altman, J. D. & Kobilka, B. K. Two functionally distinct alpha2-adrenergic receptors regulate sympathetic neurotransmission. *Nat.* **402**, 181 (1999).

31. Požgajová, M., Sachs, U. J., Hein, L. & Nieswandt, B. Reduced thrombus stability in mice lacking the α2A-adrenergic receptor. *Blood* **108**, 510–514 (2006).

32. Rouot, B., Quennedey, M. & Schwartz, J. Characteristics of the [³H]-yohimbine binding on rat brain α2. *Naunyn-Schmiedeberg's archives of pharmacology* **321**, 253–259 (1982).

33. O'Rourke, M., Blaxall, H., Iversen, L. & Bylund, D. Characterization of [³H]RX821002 binding to alpha-2 adrenergic receptor subtypes. *J. Pharmacol. Exp. Ther.* **268**, 1362–1367 (1994).

34. Smith, D. F. *et al*. Inhibition of [¹¹C]mirtazapine binding by α2-adrenoceptor antagonists studied by positron emission tomography in living porcine brain. *Synap* **59**, 463–471 (2006).

35. Staley, J. K. *et al*. Comparison of [18F]altanserin and [18F]deuteroaltanserin for PET imaging of serotonin 2a receptors in baboon brain: pharmacological studies. *Nucl. medicine biology* **28**, 271–279 (2001).

36. Riss, P. J. *et al*. Validation and quantification of [18F]altanserin binding in the rat brain using blood input and reference tissue modeling. *J. Cereb. Blood Flow & Metab.* **31**, 2334–2342 (2011).

37. Hannestad, J. *et al*. Endotoxin-induced systemic inflammation activates microglia: [¹¹C]PBR28 positron emission tomography in nonhuman primates. *Neuroimage* **63**, 232–239 (2012).

38. Jürgens, G. *et al*. Investigation into the interaction of recombinant human serum albumin with Re-lipopolysaccharide and lipid a. *J. endotoxin research* **8**, 115–126 (2002).

39. Hillmer, A. T. *et al*. Microglial depletion and activation: A [¹¹C]PBR28 PET study in nonhuman primates. *EJNMMI research* **7**, 59 (2017).

40. Hillmer, A. T. *et al*. PET imaging evaluation of [18F]DBT-10, a novel radioligand specific to α7 nicotinic acetylcholine receptors, in nonhuman primates. *Eur. journal nuclear medicine molecular imaging* **43**, 537–547 (2016).

41. Boyajian, C., Loughlin, S. & Leslie, F. Anatomical evidence for alpha-2 adrenoceptor heterogeneity: differential autoradiographic distributions of [3H]rauwolscine and [3H]idazoxan in rat brain. *J. Pharmacol. Exp. Ther.* **241**, 1079–1091 (1987).

42. Ericsson, C., Peredo, I. & Nistér, M. Optimized protein extraction from cryopreserved brain tissue samples. *Acta Oncol.* **46**, 10–20 (2007).

43. Zhang, Z., Zhao, L., Lin, Y., Yu, P. & Mao, L. Online electrochemical measurements of ca2+ and mg2+ in rat brain based on divalent cation enhancement toward electrocatalytic nadh oxidation. *Anal. chemistry* **82**, 9885–9891 (2010).

44. Brown, C., MacKinnon, A., McGrath, J., Spedding, M. & Kilpatrick, A. α2-adrenoceptor subtypes and imidazoline-like binding sites in the rat brain. *Br. journal pharmacology* **99**, 803–809 (1990).

45. Brown, C., MacKinnon, A., McGrath, J., Spedding, M. & Kilpatrick, A. Heterogeneity of α2-adrenoceptors in rat cortex but not human platelets can be defined by 8-OH-DPAT, RU24969 and methysergide. *Br. journal pharmacology* **99**, 481–486 (1990).

46. Hong, S.-S. *et al*. Bioisosteric phentolamine analogs as potent α-adrenergic antagonists. *Bioorganic & medicinal chemistry letters* **15**, 4691–4695 (2005).

47. Anzawa, N. *et al*. Increased noradrenaline release from rat preoptic area during and after sevoflurane and isoflurane anesthesia. *Can. J. Anesth. canadien d'anesthésie* **48**, 462–465 (2001).

48. Wong, D. F. *et al*. Human brain imaging of α7 nAChR with [18F]ASEM: a new PET radiotracer for neuropsychiatry and determination of drug occupancy. *Mol. Imaging Biol.* **16**, 730–738 (2014).

49. Eadie, G. On the evaluation of the constants vm and km in enzyme reactions. *Science* **116**, 688 (1952).

50. Hofstee, B. On the evaluation of the constants vm and km in enzyme reactions. *Science* **116**, 329–331 (1952).

51. Gjedde, A. Calculation of cerebral glucose phosphorylation from brain uptake of glucose analogs *in vivo*: a re-examination. *Brain Res. Rev.* **4**, 237–274 (1982).

52. Cumming, P., Léger, G. C., Kuwabara, H. & Gjedde, A. Pharmacokinetics of plasma 6-[18F] fluoro-L-3, 4-dihydroxyphenylalanine ([18F]F-DOPA) in humans. *J. Cereb. Blood Flow & Metab.* **13**, 668–675 (1993).

53. Gjedde, A., Gee, A. & Smith, D. Basic cns drug transport and binding kinetics *in vivo*. *Blood-brain Barrier Drug Deliv To CNS* 225–242 (2000).

54. Logan, J. *et al*. Graphical analysis of reversible radioligand binding from time-activity measurements applied to [N-11C-methyl]-(-)-cocaine PET studies in human subjects. *J. Cereb. Blood Flow & Metab.* **10**, 740–747 (1990).

55. Reith, J. *et al*. Blood—brain transfer and metabolism of 6-[18F] fluoro-L-DOPA in rat. *J. Cereb. Blood Flow & Metab.* **10**, 707–719 (1990).

56. Lassen, N. *et al*. Benzodiazepine receptor quantification *in vivo* in humans using [¹¹C] flumazenil and PET: application of the steady-state principle. *J. Cereb. Blood Flow & Metab.* **15**, 152–165 (1995).

57. Cunningham, V. J., Rabiner, E. A., Slifstein, M., Laruelle, M. & Gunn, R. N. Measuring drug occupancy in the absence of a reference region: the Lassen plot re-visited. *J. Cereb. Blood Flow & Metab.* **30**, 46–50 (2010).

58. Gjedde, A. & Wong, D. F. Receptor occupancy in absence of reference region. *Neuroimage* **11**, 6, S48 (2000).

59. Pearce, H. *et al.* Essential features of the P-glycoprotein pharmacophore as defined by a series of reserpine analogs that modulate multidrug resistance. *Proc. Natl. Acad. Sci.* **86**, 5128–5132 (1989).
60. Tanaka, C., Kawai, R. & Rowland, M. Dose-dependent pharmacokinetics of cyclosporin A in rats: events in tissues. *Drug metabolism disposition* **28**, 582–589 (2000).
61. Laforest, R., Longford, D., Siegel, S., Newport, D. F. & Yap, J. Performance evaluation of the microPET®-focus-f120. *IEEE Transactions on Nucl. Sci* **54**, 42–49 (2007).
62. Schiffer, W. K. *et al.* Serial microPET measures of the metabolic reaction to a microdialysis probe implant. *J. neuroscience methods* **155**, 272–284 (2006).
63. Phan, J.-A. Kiwi kinetic windows. https://github.com/jennyannphan/KiWi (2017).
64. Phan, J.-A. Kiwi kinetic windows. https://se.mathworks.com/matlabcentral/fileexchange/64128-jennyannphan-kiwi (2017).
65. Gandelman, M. S., Baldwin, R. M., Zoghbi, S. S., Zea-Ponce, Y. & Innis, R. B. Evaluation of ultrafiltration for the free-fraction determination of single photon emission computed tomography (spect) radiotracers: β-CIT, IBF, and iomazenil. *J. pharmaceutical sciences* **83**, 1014–1019 (1994).
66. Lee, H. & Blaufox, M. Blood volume in the rat. *J. Nucl. Medicine* **26**, 72–76 (1985).
67. Charlwood, P. Ultracentrifugal studies of rat, rabbit and guinea-pig serum albumins. *Biochem. J.* **78**, 163 (1961).
68. Ribas, C., Miralles, A. & Garca-Sevilla, J. A. Acceleration by chronic treatment with clorgyline of the turnover of brain α2-adrenoceptors in normotensive but not in spontaneously hypertensive rats. *Br. journal pharmacology* **110**, 99–106 (1993).

Acknowledgements

Author Contributions
J.A.P. designed, planned, and performed the experiments, analyzed data, and wrote scripts for the graphical user interface in MATLAB. A.M.L. contributed to study design, planning and assistance with image quantification. S.J. was responsible of radioligand production. D.F.W contributed to the content of the paper and interpretation of results of the study. A.G. conceived the study, designed the kinetic analyses, and supervised the work throughout the study. J.A.P. and A.G. wrote the manuscript.

Additional Information
Supplementary information accompanies this paper at https://doi.org/10.1038/s41598-017-16020-1.

Competing Interests: The authors declare that they have no competing interests.

Publisher's note: Springer Nature remains neutral with regard to jurisdictional claims in published maps and institutional affiliations.